JOURNAL OF MATERIALS SCIENCE **39** (2004) 5887– 5904

Oxidation-based materials selection for 2000°C + hypersonic aerosurfaces: Theoretical considerations and historical experience

M. M. OPEKA, I. G. TALMY, J. A. ZAYKOSKI
Naval Surface Warfare Center Carderock Division, West Bethesda, MD 20817, USA
E-mail: opekaMM@nsweed.navy.mil

Hypersonic flight involves extremely high velocities and gas temperatures with the attendant necessity for thermal protection systems (TPS). New high temperature materials are needed for these TPS systems. A systematic investigation of the thermodynamics of potential materials revealed that low oxidation rate materials, which form pure scales of SiO_2, Al_2O_3, Cr_2O_3, or BeO, cannot be utilized at temperatures of 1800°C (and above) due to disruptively high vapor pressures which arise at the interface of the base material and the scale. Vapor pressure considerations provide significant insight into the relatively good oxidation resistance of ZrB_2- and HfB_2-based materials at 2000°C and above. These materials form multi-oxide scales composed of a refractory crystalline oxide (skeleton) and a glass component, and this compositional approach is recommended for further development. The oxidation resistance of ZrB_2-SiC and other non-oxide materials is improved, to at least 1600°C, by compositional modifications which promote immiscibility in the glass component of the scale. Other candidate materials forming high temperature oxides, such as rare earth compounds, are largely unexplored for high temperature applications and may be attractive candidates for hypersonic TPS materials.

1. Introduction

The 21st century has ushered in a new, exciting era of hypersonic flight. Hypersonic flight vehicles include sub-orbital and earth-to-orbit vehicles for rapid global and space access missions. A common aspect of these future systems is the need for new high-temperature materials. Hypersonic vehicles with sharp aerosurfaces, such as engine cowl inlets, wing leading edges (LEs), and nosecaps, have projected needs for 2000 to 2400°C materials which must operate in air and be re-usable.

At this time, there are few, if any, off-the-shelf materials to meet these future hypersonic thermal protection system (TPS) needs. State-of-the-Art high temperature materials include carbon-carbon composites (C-C) and silicon carbide-based (SiC) composites, such as C-SiC and SiC-SiC. Ultra-High-Temperature Ceramics (UHTCs), such as $Zr(Hf)B_2$-SiC, are being developed but are less mature at this time. Carbon-carbon composites have very high temperature structural capabilities but are not oxidation-resistant. Coatings have been and are being developed for oxidation-resistance, but cyclic life capabilities are modest due to the difficulties of managing the thermal expansion coefficient (CTE) mismatch between the C-C composite and the coating systems. The SiC-based composites exhibit oxidation resistance up to 1600°C in hypersonic environments, but thermal cycling lifetimes are also modest due to CTE- mismatch-induced matrix cracking which allows direct oxidation of the carbon fiber reinforcement. The UHTCs, based on the diborides of zirconium and hafnium, have exhibited relatively good oxidation resistance above 1600°C. The oxidation mechanisms of these materials are not well understood. Recent Navy efforts to understand UHTC oxidation mechanisms, and to develop new, highly oxidation-resistant 2000°C materials, are presented here. This paper describes prior development of ultra-high-temperature, oxidation-resistant materials; thermodynamics and kinetics principles related to oxidation; theoretical aspects of the oxidation of UHTC materials; and experimental results associated with compositional variations of UHTC materials.

2. Developmental history

Distinct lines of research have contributed significantly to our current understanding of oxidation-resistant ultra-high temperature materials: coating systems for refractory metals and subsequent development of oxidation-resistant intermetallic compounds, oxidation-resistant graphite compositions, and the development of boride-based UHTCs.

The structural usefulness of refractory metals, and their lack of high temperature oxidation-resistance, motivated the pursuit of oxidation-resistant coatings. Considerable research was conducted, especially in the

1960s, and a number of texts summarizing the developments are available [1–5]. Although a broad range of materials was investigated, a significant proportion of the work was based on compositions containing silicon (Si), aluminum (Al), and chromium (Cr). Packer [6] summarized research on silicides, and an important conclusion is the significance of low pressure and high temperature environments on limiting the life of such materials and coatings. Perkins and Packer [7] identified the maximum temperature capability of $MoSi_2$ coatings as 1800°C in atmospheric pressure (hypersonic) environments. Recent research on the oxidation of intermetallics, especially emphasizing aluminides for gas turbine applications, has been compiled by Grobstein and Doychak [8].

Oxidation-resistant graphite compositions were developed in parallel with refractory metal coatings in the 1960s [9, 10]. One of the most important compositions, designated "grade JTA" graphite [9], was optimized for oxidation resistance at 2000°C. It used additions of ZrB_2 and Si (balance carbon) at an approximately 50 weight percent basis. Further optimization using transition metal additions (e.g., niobium) were found to improve oxidation performance at high temperatures, but with the penalty of poorer performance at lower temperatures. Krivoshein and coworkers [11] reported that Nb additions (10 wt%) improved oxidation performance of ZrB_2-SiC modified graphite, but that *V* additions at the same level provided maximum improvement.

Significant research was reported on the refractory boride compounds beginning in the late 1940s with crystal structure [12] and melting point [13] measurements. An initial survey of the oxidation resistance of transition metal diborides up to 1500°C revealed that the group IVb compounds were the most resistant [14]. A survey of oxidation resistance of the diborides of Hf, Zr, Ti, Ta, and Nb from 1200 to 2200°C (inductively heated samples in flowing He-O_2 mixtures) also revealed that HfB_2 was the most oxidation resistant, followed by ZrB_2. The temperature dependence of the oxidation data for both compounds indicated significant rate changes at the respective metal oxide phase transition temperatures [15]. Oxidation testing in flowing He-O_2 mixtures with H_2O (at 613 Pa) exhibited a five-fold increase in oxidation rate of HfB_2 at 933°C versus the nominal dry He-O_2. Similar oxidation measurements at 1487°C showed no rate difference [16]. Additional oxidation studies on ZrB_2 and HfB_2 demonstrated that metal-rich compositions (e.g., $HfB_{1.7}$) oxidized at lower rates (by up to a factor of 50) versus boron-rich compositions (e.g., $HfB_{2.12}$) [16].

Numerous investigations to improve the oxidation resistance of ZrB_2 and HfB_2 have been reported [17–20]. Compositions with 5 to 50 vol% SiC were investigated for both ZrB_2 and HfB_2 over a wide range of test temperatures and pressures; 20 vol% compositions were judged optimal for hypersonic vehicles in a series of efforts supported by the US Air Force [16, 19, 21–23]. Additions of C (5, 10, 15, 20, 30, and 50 vol%) improved thermal stress resistance, but were detrimental to oxidation resistance at all proportions. Additions of Cr (10 mol%), Al (20 mol%), and Ta (30 mol%) were found to be detrimental to oxidation resistance. An addition of 4 vol% of a Hf-20 at.%Ta alloy had no effect on the oxidation properties, although the metal phase was converted to the carbides during the hot-press fabrication process. Excess Hf metal additions to produce a 50 mol% HfB_2 + 50 mol% HfB composition exhibited rapid, preferential oxidation of the HfB phase. Additions of silicon to substitute on the boron sub-lattice yielded a HfB_2 + "HfSi" skeletal phase which also exhibited rapid, preferential oxidation. (It is noted here that "HfSi" was identified by X-ray diffraction; other Hf-Si or Zr-Si second phases are possible, but have not been explored for oxidation response.) Additions of SiB_6 (10 and 20 vol%) were found to increase oxidation resistance, but were not superior to SiC additions.

Other systematic studies of additions into ZrB_2 and or HfB_2 have been conducted. Shaffer [24] evaluated the oxidation resistance of ZrB_2 with additions of the disilicides of Ta, Nb, W, Mo, Zr, $Mo_{0.5}Ta_{0.5}$, and $Mo_{0.8}Ta_{0.2}$, as well as Zr_5Si_3. The additive amounts were not specified, however, and only the conclusion was stated that $MoSi_2$ was "unquestionably the best." Additional oxidation experiments with varying proportions of $MoSi_2$ (1 to 20 mol%) were conducted at 1950°C and revealed the optimum composition to be 10 mol%. The ZrB_2 + 10 mol%$MoSi_2$ composition was marketed by the Carborundum Company (US) under the Trade name "Boride Z".

Pastor and Meyer [25] evaluated the oxidation resistance of ZrB_2 with additions of MSi_2 or M_5Si_3, where M is a transition metal Zr, Ta, Cr, Mo, or W. On the basis of scale thickness measurements after oxidation testing for up to 100 h at 1200 and 1400°C, the ZrB_2 + 15 wt%$CrSi_2$ composition was found to be the most oxidation resistant.

Lavrenko and coworkers [26] reported that a ZrB_2 + 50 wt%$ZrSi_2$ composition was more oxidation resistant than $MoSi_2$ and WSi_2, and could be used up to 1700°C. However, since oxidation data only up to 1200°C are reported, it is not clear how the conclusion is supported.

The oxidation kinetics mechanism(s) of the diboride-based materials are only partly understood despite significant research. Oxidation kinetics measurements are typically based on weight change or scale thickness changes with time upon exposure to a known temperature and oxidizing atmosphere. However, weight change and scale thickness measurements are confounded by simultaneous oxidation and vaporization (of BO_x vapor species) processes. Total oxygen consumption measurements (per unit area of sample) have been utilized to overcome this limitation [27].

Initial oxidation studies were conducted in 1955 on porous ZrB_2 samples from 649 to 1315°C [28]. The oxidation kinetics were found to be parabolic, the rates increased with oxygen partial pressure, and the presence of H_2O also increased the oxidation rate.

Berkowitz-Mattuck measured total oxygen consumption for ZrB_2 over a higher temperature range (1200–1530°C) and a lower oxygen partial pressure (P_{O_2}) range (1070 to 5200 Pa) in helium (He) at 1.01×10^5 Pa total pressure [27]. Parabolic rate kinetics were

also observed, as were modest increases in oxidation rates with increasing P_{O_2}. From metallographic examination of tested samples, it was concluded that oxidation proceeded by inward diffusion of oxygen, and it was suggested that oxygen diffusion through ZrO_2 was the rate controlling step.

Kuriakose and Margrave measured weight changes for ZrB_2 over the temperature range of 945–1256°C and also reported parabolic oxidation kinetics [27, 29]. At 1056°C they observed that the parabolic rate constant increased directly proportional to P_{O_2} (range was 1.36×10^4 to 9.92×10^5 Pa at 1.01×10^5 Pa total pressure with balance He). Berkowitz-Mattuck extended the oxidation kinetics studies of ZrB_2 to understand the change in P_{O_2} dependence with temperature [30, 31]. The P_{O_2} dependence was confirmed at a test temperature of 927°C, but no dependence was found at 1557°C. Additional testing also revealed a significant change in the activation energy at 1057°C, changing from 20 kcal/mole below this temperature to 70 kcal/mole above it. Abrupt changes in the oxidation rate kinetics were also observed at the temperatures corresponding to the monoclinic to tetragonal oxide phase transitions for both ZrB_2 and HfB_2.

Other oxidation studies have been conducted on the oxidation kinetics of ZrB_2, HfB_2, and their respective SiC-modified compositions [32–40]. Oxygen diffusion through the B_2O_3 liquid phase was identified as the rate limiting step associated with oxidation of the pure diborides up to approximately 1200°C. Above this temperature, the increased oxidation rates were attributed to oxygen transport through the ZrO_2 or HfO_2 phase. The addition of SiC was found to significantly increase the temperature range of the glass as the primary oxygen barrier. A two layer scale was observed to form with HfO_2 inner and SiO_2 outer components. The reduction in oxidation rate was observed above 1350°C. Below this temperature, SiC inclusions are found in the HfO_2 scale since the SiC particles do not oxidize significantly to generate the SiO_2 glass component [34].

Low temperature oxidation studies have also been conducted for these borides. Preferential oxidation of the Zr or Hf at 500°C at an oxygen pressure of 1.3×10^{-3} Pa has been reported. Boron inclusions, which coalesced into layers, were observed in the oxide scale. Solution of oxygen into the diboride lattice was also reported [36]. Changes in the oxidation mechanism were noted at approximately 500°C [37].

In addition to the diborides, other materials were investigated for potential hypersonic applications [20, 41–44]. Materials based on ZrC and HfC were extensively studied, but were found to oxidize (non-protectively) below 1800°C, which eliminated them from consideration for the temperature cycling hypersonic applications. Additions of SiC did not solve the rapid oxidation at low-temperatures. Hafnium-tantalum alloys (e.g., Hf-20 at.%Ta) were found to exhibit good oxidation behavior, but were limited by the relatively low melting point of 2000°C at this composition. Iridium coatings on graphite were also evaluated, but were judged costly and not sufficiently refractory due to the Ir-C eutectic at 2296°C. The viscosity of SiO_2 was significantly increased by the addition of W powder in 10 and 20 vol% additions. These materials exhibited increased sensitivity to thermal stress failure and deformed by viscous flow into blunt shapes. Since hypersonic applications typically require the high temperature materials to retain sharp radii for leading edges and propulsion inlets, this shape change was unacceptable. By the early-1970s, the ZrB_2- and HfB_2-based materials were identified to be the most promising for hypersonic applications with cyclic exposure from ambient temperature up to 2700°C [18, 41, 42].

Prior materials development for hypersonic applications does not include significant emphasis on oxide materials. They have not been pursued for these applications due to the demanding structural and thermostructural requirements of such systems, and low thermal shock resistance of oxides in general. It must be asked whether the optimized choice of hypersonic materials should be oxide or non-oxide materials. Oxide materials are, at best, intrinsically resistant to oxidation. However, oxide-oxide composites for 2000°C usage do not currently exist, and current and developmental oxide composites for aircraft applications cannot be used to that temperature. Such ultra-high-temperature oxide composites will likely be very costly due to the need to develop new creep-resistant reinforcements and suitable fiber-matrix interface materials to evade brittle fracture behavior. In addition, oxides and oxide composites incur significant design penalties due to their relatively high CTE and stiffness, and low thermal conductivity. Such a new 2000°C oxide composite would have to be developed for dedicated hypersonic application at very high cost. However, the payoff of intrinsic oxidation resistance requires a continuing look into oxide materials for these applications.

The materials selection process presented here addresses the optimization of non-oxide ceramic compositions for high temperature hypersonic applications.

3. Oxidation-thermodynamics and kinetics

The selection of new oxidation-resistant materials is based on chemical thermodynamics and kinetics. Chemical thermodynamics is a powerful tool for identifying the equilibrium phases associated with the oxidation kinetics process(es). Chemical thermodynamics can be seen as providing the boundary conditions for understanding the oxidation kinetics processes. The thermodynamics-based calculations provided in this paper are based on the following relation:

$$\Delta G = \Delta G^{\circ} + R \cdot T \cdot \ln(Q) \tag{1}$$

where ΔG is the change in Gibbs Free Energy (superscript refers to standard state) associated with a given chemical reaction, R is the ideal gas constant, T is the reaction temperature, and Q is the activity quotient [45, 46]. At the condition of chemical equilibrium, ΔG is zero and Equation 1 reduces to:

$$\Delta G^{\circ} = -R \cdot T \cdot \ln(k) \tag{2}$$

or,

$$\Delta G^{\circ} = -2.303 \cdot R \cdot T \cdot \log(k) \qquad (3)$$

where k is the reaction equilibrium constant. Gibbs Free Energies of Formation (FEOF) at standard state (ΔG_f^0) have been measured, and/or estimated, and tabulated as a function of temperature for many compounds of interest [47–50].

3.1. Thermodynamics and condensed phase equilibria

A stability diagram (Fig. 1) showing regions of metal and condensed metal oxide equilibria using Equation 3 was constructed for the elements Be, Y, Hf, Ta, W, Re, and Ir. These elements were selected as the most refractory representatives of their respective columns or groups in the periodic chart of elements. The diagram provides the metal-metal oxide equilibria as functions of temperature and oxygen pressure, P_{O_2}. Each metal is stable below its respective metal-metal oxide equilibrium line, while the condensed oxide is stable above the equilibrium line. This diagram allows the generalized hypersonic environment to be directly compared with the metal-metal oxide stability regions.

The FEOF data for BeO, HfO_2, Ta_2O_5, and Re_2O_7 were taken from Schick [47], for WO_3 from "JANAF" [48] , for Y_2O_3 from Pankratz [49], and for IrO_2 from Knacke [50]. As necessary, FEOF were extrapolated linearly from the highest temperature data available. For Y_2O_3, WO_3, Re_2O_7, and IrO_2, the data were extrapolated above 1723, 2723, 361, and 1027°C, respectively, to compare with the hypersonic vehicle environment. Multiple condensed oxides exist and were considered for W (WO_2 and WO_3) and Re (ReO_2, ReO_3, and Re_2O_7). For both metals, the suboxides (WO_2, ReO_2, and ReO_3) decompose below 1500°C and were neglected.

The hypersonic environment envelope divides the diagram of Fig. 1 into three distinct groups of elements. The first group includes noble metals, such as iridium (Ir), for which the metal is the equilibrium condensed phase in the hypersonic environment. Since a condensed oxide does not form, mass loss from Ir_xO_y vapor species must be considered. Oxidation mass loss rates for Ir are extremely low [51–53]. Other possible noble elements include rhodium, platinum, palladium, osmium, ruthenium, gold, and silver, which are not shown. Osmium and Ru exhibit very high mass loss rates in oxidizing environments [53]. Of the remaining elements, only iridium, and possibly rhodium, have melting points high enough to be considered for hypersonics applications. They should be considered for development but are not discussed further in this paper.

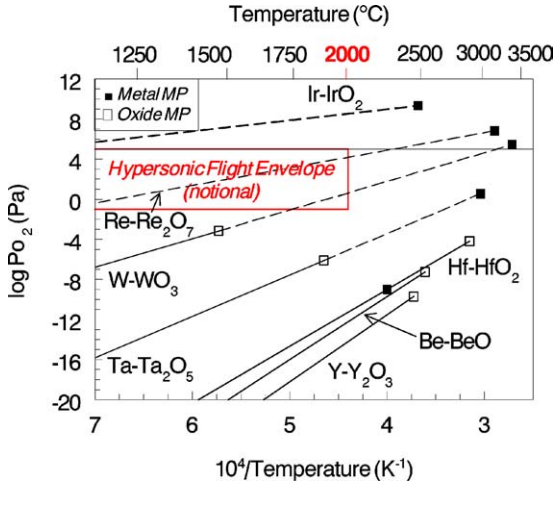

Figure 1 Metal-metal oxide condensed phase equilibrium diagram.

The second element group shown in Fig. 1 includes those elements which form condensed oxides in the hypersonic environment, but the oxide melting point is below the 2000°C upper use temperature. These elements include tantalum, tungsten, rhenium, and by analogy, aluminum, titanium, molybdenum and all other group Vb (vanadium, niobium) and VIIb (manganese, technetium) elements. Since the oxides of these elements have relatively low melting points and melt viscosities, aerodynamic shear forces would remove them quickly and high ablation rates would be observed. In addition to the low oxide melting point limitation, these metals oxidize and experience high mass loss rates (from oxidative vaporization) at modest to high temperatures. Oxidation rates for Ta and W (as well as for Nb and Mo) have been reviewed by Kofstad [54]. High oxidation rates for Re in air are reported in the 300 to 1500°C temperature range [55, 56].

The third group, hafnium (Hf), yttrium (Y), and beryllium (Be), includes those elements which exist only as solid, condensed oxides throughout the hypersonic environment. Although only these three elements are shown, the result may be generalized to include zirconium, chromium, silicon, scandium, and the rare earth metals. Silicon is also included in this group because of the high viscosity of the molten oxide. Since these elements have melting points near to or lower than 2000°C, they have to be used as refractory compounds (silicides, borides, carbides, nitrides, etc.).

Thus, initial candidate hypersonic materials include noble, refractory metals (Ir and/or Rh), and compounds (based on Zr, Hf, Be, Si, Y, Sc, and rare earths) which form refractory oxides.

3.2. Oxidation kinetics

While equilibrium thermodynamics provides an important foundation for materials selection, a second foundation is oxidation kinetics. For hypersonic applications, materials with a low oxidation rate are required. The need for higher temperature gas turbine materials has motivated significant investigations into very low oxidation rate materials. As shown in Fig. 2, Zr and Hf exhibit relatively high oxidation rates, while the most slowly oxidizing materials at high temperatures are those which form scales composed of pure SiO_2, Al_2O_3, Cr_2O_3, or BeO [57–64]. Above approximately 1100°C, SiO_2 scale-forming materials (SiC, Si_3N_4, $MoSi_2$, and possibly other silicides) have the lowest known oxidation rates [65, 66]. Beryllides (e.g., Ta_2Be_{17} and $ZrBe_{13}$) have very low oxidation rates up to 1250°C, but the rates increase rapidly with temperature [62, 63].

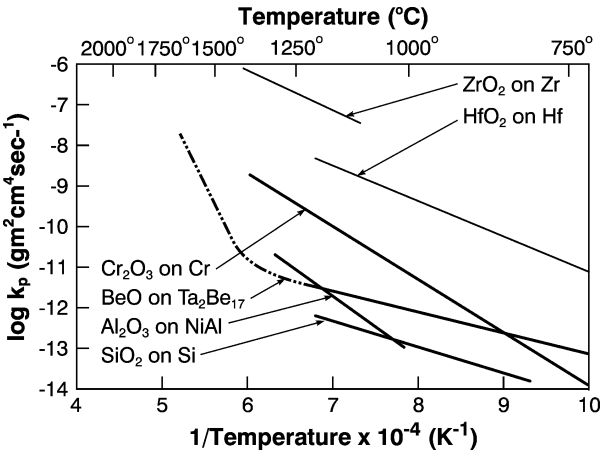

Figure 2 Parabolic oxidation rate constants for various metals and compounds.

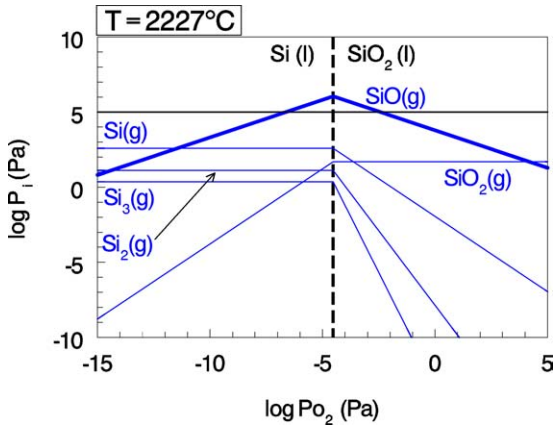

Figure 3 Volatility diagram for Si-SiO_2 system at 2227°C.

3.3. Thermodynamics and vapor phase equilibria

Equation 3 may also be employed to construct diagrams of the vapor pressures of metal and metal oxide gaseous species as a function of oxidant pressure. Such a vapor phase diagram [67, 68], or volatility diagram, for the silicon-oxygen (Si-O) system at 2227°C is shown in Fig. 3. The vertical dashed line, at an oxygen pressure (P_{O_2}) of 3.0×10^{-5} Pa, is the equilibrium line defined by the reaction:

$$\mathrm{Si(c,\,l) + O_2(g) \rightarrow SiO_2(l)} \qquad (4)$$

and separates the diagram into the two regions in which condensed Si and SiO_2 exist. Unit activity is assumed for both Si and SiO_2, which is typical for this type diagram. Other lines show the vapor pressures of the Si-O gaseous species (Si, Si_2, Si_3, SiO, SiO_2) as a function of P_{O_2}. The diagram may be seen as a schematic of the vapor pressure changes from the external surface of the SiO_2 scale (right side of diagram) on oxidized Si, to the interior of the Si (left side of the diagram).

It should be noted that the vapor pressures are highest at the Si-SiO_2 interface (SiO vapor) and not at the exterior surface of the SiO_2. This high interfacial vapor pressure limits the use temperature of SiO_2-forming materials. The SiO_2 scale is continuously ruptured when the interfacial (SiO) pressure exceeds ambient pressure and the scale loses its protective capability. At this condition, the SiO_2 scale is consumed via the reaction:

$$\mathrm{Si(l) + SiO_2(l) \rightarrow 2SiO(g)} \qquad (5)$$

The SiO(g) diffuses outward from the base of the porous SiO_2(l) scale and reacts with O_2(g) to form SiO_2(l), either within the scale or as smoke outside the scale [68]. If the SiO_2 scale is entirely consumed (or if not formed initially), oxidation proceeds via the reaction:

$$\mathrm{Si(l) + 1/2O_2(g) \rightarrow SiO(g)} \qquad (6)$$

The conditions represented by reactions (5) and (6) yield rapid oxidation of the Si. Wagner first showed that the transition between the rapid, (active) oxidation of Si(c,l) which occurs via reaction (6) and the slow (passive) oxidation via reaction (4) was governed primarily by the thermodynamics of the system [69]. Gulbransen includes reaction (5) in his description of active oxidation [68], although other researchers have restricted the term to describe the effect of reaction (6) only [70, 71].

The maximum in P_{SiO} at the Si-SiO_2 interface uniformly increases with temperature. The calculated SiO interfacial vapor pressure exceeds 1.01×10^5 Pa at 1865°C as shown in Table I.

TABLE I Calculated vapor pressures for oxides

Material	Condensed oxide	Oxide type	Melt temp (deg C)	Dominant vapor species (at Interface)	log P_{MOx} at 1727°C (Pa)	log P_{MOx} at 2227°C (Pa)	Temp (deg C) for $P = 10^{-4}$Pa	Temp (deg C) for $P = 10^{5}$Pa
O_2 Barrier matls								
Be	BeO	Crystalline	2550	Be	2.85	4.43	820	2495
Si	SiO_2	Amorphous	1725	SiO	4.5	6.06	750	1865
Al	Al_2O_3	Crystalline	2040	Al, Al_2O	2.87	4.42	800	2490
Cr	Cr_2O_3	Crystalline	2300	Cr	2.14	3.9	970	2690
B	B_2O_3	Amorphous	450	B_2O_3, B_2O_2	4.11	5.88	800	1950
Scale structures								
Be	BeO	Crystalline	2550	Be	2.85	4.43	820	2495
Sc	Sc_2O_3	Crystalline	2400	Sc	2.02	3.8	950	2750
Y	Y_2O_3	Crystalline	2430	Y	0.626	2.63	1120	3330
Zr	ZrO_2	Crystalline	2700	ZrO	−2.18	0.926	1520	3640
Hf	HfO_2	Crystalline	2800	HfO	−2.58	0.506	1570	3670
Ta	Ta_2O_5	Crystalline	1890	TaO_2	−1.92	0.926	1490	3730

Gulbransen *et al.* [72] confirmed the active-passive transition boundary line for elemental Si in the 1100 to 1300°C temperature range. Extrapolating these experiments to air at 1.01×10^5 Pa yields the onset of active oxidation of Si at 1660°C.

Interfacial vapor pressures have also been calculated for the Si compounds of interest. For SiC, interfacial vapor pressures have been calculated assuming the bounding cases of unit Si and unit C activity. These activity values result in 1.01×10^5 Pa interfacial pressure (sum of all vapor species) at temperatures of approximately 1800 and 1515°C, respectively. Calculations for Si_3N_4 yield a 1.01×10^5 Pa interfacial pressure at 1790°C for the case of unit Si activity. For $MoSi_2$, 1.01×10^5 Pa interfacial vapor pressure is predicted to occur at 1850°C for the case of unit Si activity [73]. Experimental data for these three SiO_2-forming compounds have shown reasonable agreement with predictions [74–77].

It is not clear that the equilibrium interfacial vapor pressure for any pure SiO_2-forming compound can be low enough to significantly increase the use temperature above approximately 1800°C (Jacobsen [65] has set the temperature limit at approximately 1725°C). Improved performance appears to be possible only by reducing the Si activity. This path, however, is limited since a lower Si activity will introduce additional components to the oxide scale and compromise the protective capability of pure SiO_2. It is emphasized here that this approximate 1800°C temperature limit is based on thermochemical quantities, and not on oxidation kinetics.

It is conceivable that the other slow-growing oxides (based on Al, Cr, and Be) could have interfacial vapor pressures that are lower than for Si at high temperatures. Volatility diagrams for the Al-Al_2O_3, Cr-Cr_2O_3, and Be-BeO systems at 2227°C are shown in Figs 4–6, respectively ("JANAF" thermodynamic data [48] were used for all three metals). The diagrams reveal that the highest vapor pressures for these systems also exist at the metal-oxide interface. The vapor pressures for Al, Cr, and Be reach 1.01×10^5 Pa at 2490, 2690, and 2495°C, respectively. The vapor pressures were also computed as a function of temperature and are summarized in Table I.

However, oxidation studies for materials based on these metals or compounds have revealed lower temperature limits than those imposed by the 1.01×10^5 Pa interfacial pressure. In isothermal oxidation of Cr at 980°C, an oxide scale was grown separated from the metal surface [78]. The scale grew by metal vapor transport from the oxide-free metal surface to the interior of the detached scale. Both Cr and Al have exhibited similar oxide scale disruption resulting from the high metal vapor pressures beneath the scale [79]. Oxidation data for beryllides show that protective scales have not been observed above 1650°C [80]. An interfacial vapor pressure of 10^{-4} Pa has been reported to be sufficient to disrupt protective oxide scale formation [68, 77]. Table I also provides the calculated temperatures for which the interfacial vapor pressure is 10^{-4} Pa. It is noted that these temperatures, 750°C for Si up to 970°C for Cr, are very low relative to the desired 2000°C capability.

The SiO_2-forming materials may be operated up to a 1.01×10^5 Pa interfacial vapor pressure (1800°C), yet Cr_2O_3-formers show unusual oxidation scaling behavior even at the interfacial pressure of 10^{-4} Pa (at 980°C). This may be explained, in part, by the differences in the mass transport mechanisms of the condensed oxides. The growth of SiO_2-scales has been correlated to the transport rate of molecular oxygen (O_2) [65, 66, 80, 81]. The open structure of SiO_2 glass also allows oxidation products (SiO, CO) at modest pressures to move outward without failure of the protective scale. Only when the interfacial pressure of these product species approaches 1 atm (or a lower pressure ambient environment for hypersonic applications), the

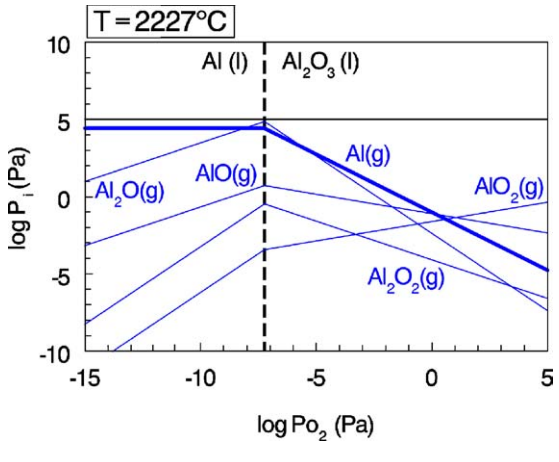

Figure 4 Volatility diagram for Al-Al_2O_3 system at 2227°C.

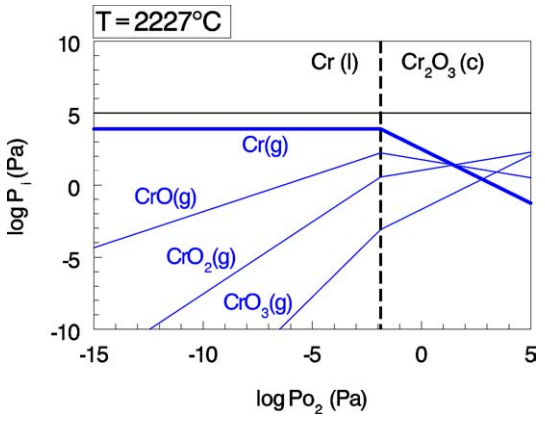

Figure 5 Volatility diagram for Cr-Cr_2O_3 system at 2227°C.

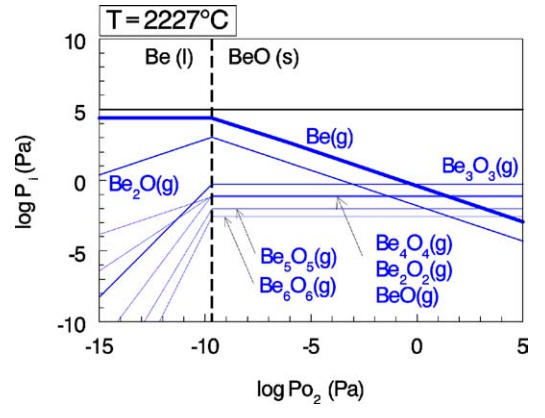

Figure 6 Volatility diagram for Be-BeO system at 2227°C.

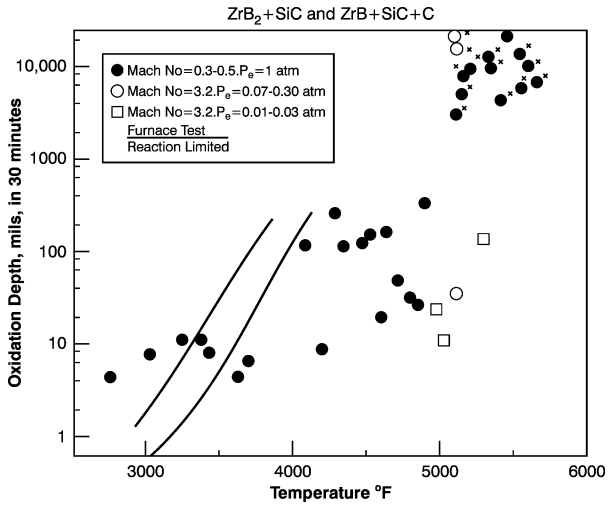

Figure 7 Arc-heater and furnace oxidation scale thickness versus temperature results for ZrB_2-SiC.

system experiences disruptive degradation of the protective scale. For Al, Cr, and Be, the oxide scale is crystalline, which generally allows only ionic transport. For these metals, oxide scale growth includes, as a significant diffusion mechanism, metal cations diffusing outward from the metal-oxide interface to the oxide scale outer surface. Since molecular vapor species do not diffuse easily through a compact oxide scale, the scale is disrupted at relatively low vapor pressures. By this reasoning, materials that form a glass component in the scale are better choices for high temperature environments since they are more structurally tolerant of high interfacial vapor pressures.

4. Theoretical aspects of the oxidation of boride materials

The UHTC materials based on mixtures of the ZrB_2 or HfB_2 and SiC have exhibited relatively good oxidation behavior in arc-heater testing up to the melting points of the base materials. Additionally, the oxidation data shown in Fig. 7 [82] do not reveal a catastrophic increase in oxidation rate from increasing interfacial vapor pressures.

Fig. 8 shows a Scanning Electron Microscopy (SEM)/Energy Dispersive Spectroscopy (EDS) analysis of the oxide scale cross-section on a $ZrB_2 + 20$ vol% SiC ceramic sample after furnace oxidation at 1600°C in air for 2 h. The backscatter image reveals the two phases (ZrB_2, SiC) in the unoxidized zone at the bottom of the photo. The EDS analysis reveals the presence of Zr and Si through the base material (the distribution of B and C were not conclusively identified by this EDS analysis). In the oxidized regions (four upper zones of the photo), Zr is the dominant element at the base of the scale, while the Si is the dominant element at the scale surface.

Volatility diagrams provide insight into the oxidation response of these ZrB_2 + 20 vol% SiC materials. The diagram for the B-B_2O_3 system at 2227°C is shown in Fig. 9. The system is unique for the lack of a peak pressure at the B-B_2O_3 interface, and for the constant pressure through the oxide scale, compared to the Si-SiO_2, Al-Al_2O_3, Cr-Cr_2O_3, and Be-BeO systems (Figs 3–6).

The volatility diagram for the Zr-ZrO_2 system at 2227°C is shown in Fig. 10. The diagram is very similar

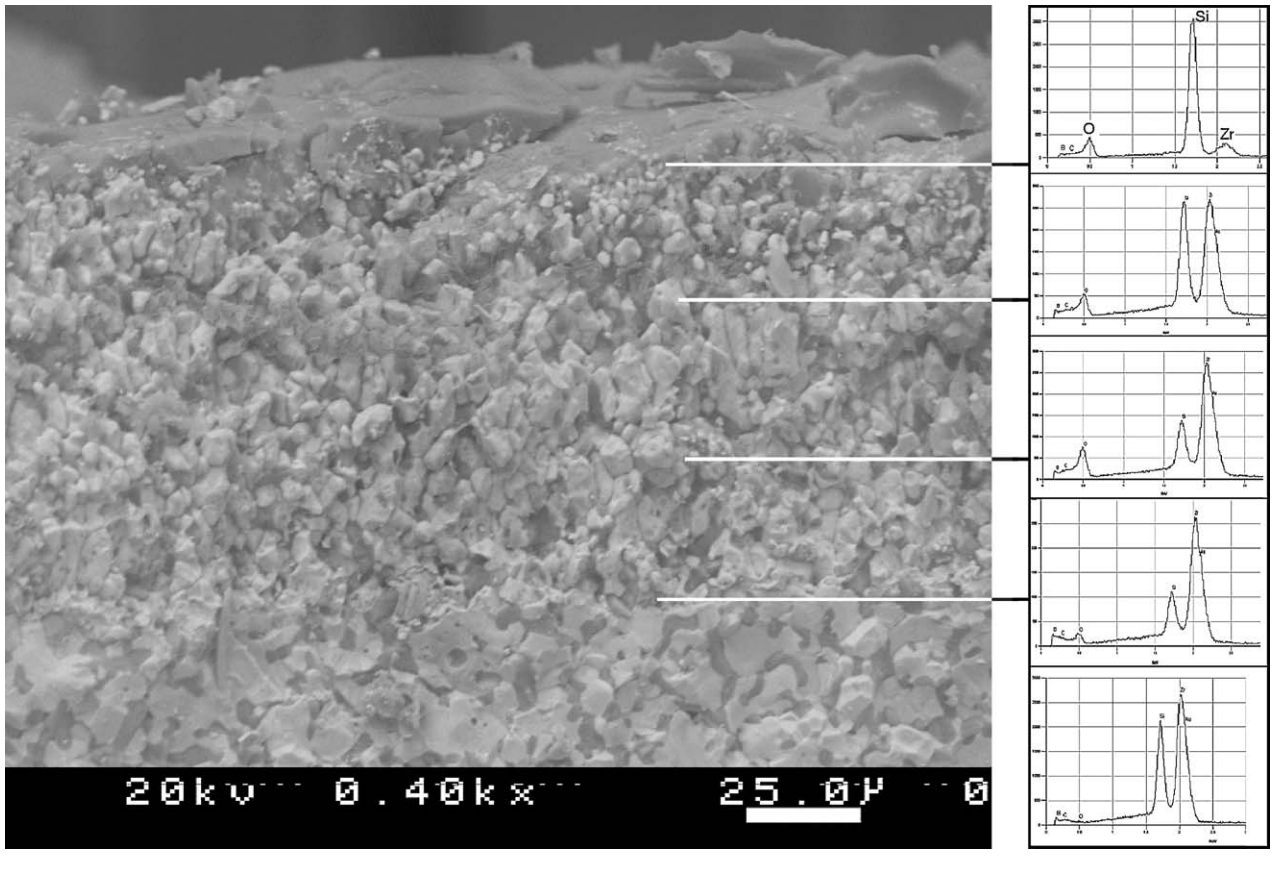

Figure 8 Microstructure and elemental distribution in ZrB_2-SiC ceramics furnace-oxidized at 1600°C for 2 h.

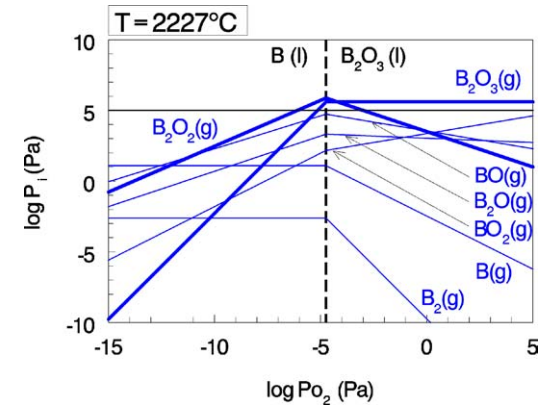

Figure 9 Volatility diagram for B-B_2O_3 system at 2227°C.

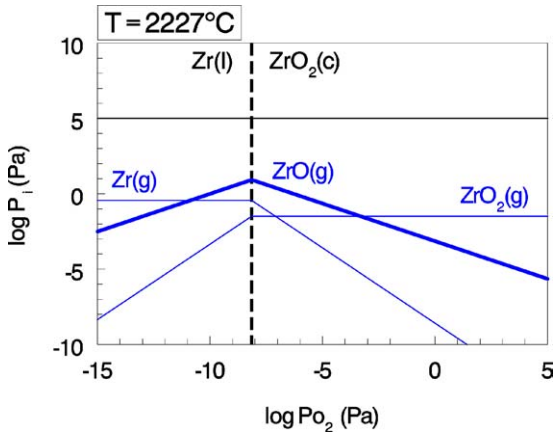

Figure 10 Volatility diagram for Zr-ZrO_2 system at 2227°C.

to that for Si-SiO_2 (Fig. 3), but exhibits significantly lower vapor pressures for all species. The maximum vapor pressure is found at the metal-metal oxide interface, but is of the order of 10 Pa compared to approximately 10^6 Pa for the Si-SiO_2 interface.

A combined volatility diagram of the Zr-ZrO_2, Si-SiO_2, and B-B_2O_3 systems at 2227°C is shown in Fig. 11. The vapor pressure magnitudes will differ for the ZrB_2 + 20 vol%SiC ceramics since unit activities are assumed for the calculation shown by Fig. 11.

The diagram reveals significant insights into the behavior of these materials. The vapor pressures associated with Zr (and Hf) are low enough to sustain an adherent oxide scale, which is confirmed by arc-heater testing. The pressures associated with B_2O_3, although high, will be significantly lower due to the reduced B activity in the ZrB_2 or HfB_2 [83]. In addition, in a temperature gradient environment, such as in an arc-heater test (815°C gradients have been measured across a 2.5 mm scale thickness [82]) or on a hypersonic leading edge, the B_2O_3 vapor pressure will continuously decrease from the scale surface inward. Boria evaporation will then occur from the outer surface and will not catastrophically disrupt the oxide scale. Due to these temperature and pressure gradients, oxidation rates in arc heater testing are significantly lower, by up to 90% at 2200°C, than those measured using RF heating techniques [16, 19, 21]. This significant difference is also expected between arc-heater testing and furnace testing.

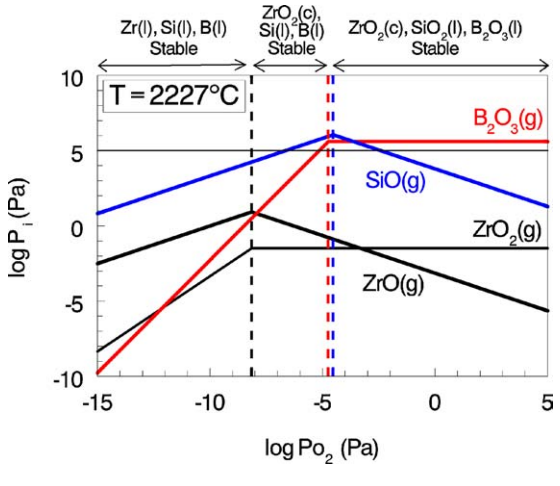

Figure 11 Combined volatility diagram for Zr-ZrO_2, Si-SiO_2, and B-B_2O_3 systems at 2227°C.

The substantial temperature and B_xO_y vapor pressure gradients through the scale promotes the retention of liquid B_2O_3 in the scale even to very high surface temperatures. Additionally, the B_2O_3(l) wets the ZrO_2 scale and persists due to the high surface energy of ZrO_2. At 1400°C, 10% of the B_2O_3(l) formed is retained in the scale on pure ZrB_2 [84]. For the ZrB_2-SiC ceramics, this retained B_2O_3 content is much higher due to formation of borosilicate glass.

Gaseous SiO forms at the scale interface from SiC and migrates outward. Since O_2 pressure also increases outward, SiO re-oxidizes to form condensed SiO_2 at the exterior of the scale where it combines with B_2O_3 to form borosilicate glass. Since the B_2O_3 preferentially evaporates from the scale surface, the outer glass becomes enriched with SiO_2. The ZrO_2 skeleton provides a framework for the glass to be retained and not removed by shear forces. The application use temperature of this materials system appears to be limited by melting of the oxide scale and/or the base material than by disruptively high interfacial vapor pressures [19, 21, 82]. Thus, these ZrB_2-SiC (and HfB_2-SiC) UHTC materials provide relatively good oxidation resistance by forming thermodynamically compatible oxide scale components. This scale system mitigates the effects of, or recovers from, high interfacial vapor pressures.

However, the protection gained by the formation of the exterior SiO_2 layer also provides the condition for P_{SiO} to increase and become disruptive. As the SiO_2-rich glass increases in thickness, O_2 transport decreases, O_2 pressure beneath the glass layer decreases, and P_{SiO} increases until the glass layer is ruptured. New formation of SiO_2 from SiO vapor suggests a cyclic protective/non-protective scale-forming sequence. A semi-protective scale should result, and this mechanism change in oxidation kinetics should be observed above the SiC-SiO_2 active-passive transition temperature. It is not clear that this cyclic, semi-protective oxidation behavior has been observed to-date.

The correlation between oxidation kinetics and oxygen transport mechanisms is not fully understood at this time. Up to approximately 1200°C, the parabolic rate constants for the oxidation of ZrB_2 vary linearly with

P_{O_2}, which affirms that molecular O_2 transport through the B_2O_3 glass is the rate limiting step. Above 1200°C, the rate constants exhibit no dependence on P_{O_2}, which is expected if oxygen transport through ZrO_2 is the rate limiting step [79]. The addition of SiC has the effect of increasing the temperature for which glass transport properties provide the rate limiting step. The role of oxygen transport through the crystalline ZrO_2 skeleton in ZrB_2 + SiC materials is not clear at this time.

Compositional variations, which form glasses that are stable to higher temperatures, and have low O_2 diffusion rates and low vapor pressures, could further improve the oxidation resistance of these materials. Glasses have been identified which are composed of refractory oxides (La_2O_3, ZrO_2, ThO_2, Ta_2O_5, TiO_2, WO_3, and B_2O_3) [85]. It is recommended that new UHTC materials which exploit these glass-forming compositions be investigated.

Compositional variations, which reduce oxygen transport through the skeleton phase, may improve the oxidation resistance as well. It is known that additions of higher valence metals into the ZrO_2 lattice will reduce oxygen vacancy concentration and diffusion [79]. The pyrochlore phases associated with ZrO_2 and rare earth oxides are also known to exhibit significantly lower oxygen diffusion than ZrO_2, as shown in Figs 12 and 13 [86, 87]. The *in-situ* formation of pyrochlore phases in UHTCs, and subsequent oxidation behavior, has not been investigated. It is recommended that new UHTC materials with rare earth additions be investigated. Vapor pressures at the metal-metal oxide interface are compared in Table I for potential skeleton phase-formers including Zr, Hf, Sc, Y, Be, and Ta. Materials forming HfO_2 and ZrO_2 are the best materials from this interfacial vapor pressure criterion.

The carbides and nitrides of Zr (and Hf) are inferior to the diborides in oxidation behavior. Arc-heater testing of the carbides of Zr and Hf has been conducted at temperatures of 2400 to 2700°C with exposure times of 30 to 180 s in a gas environment replicating stoichiometric

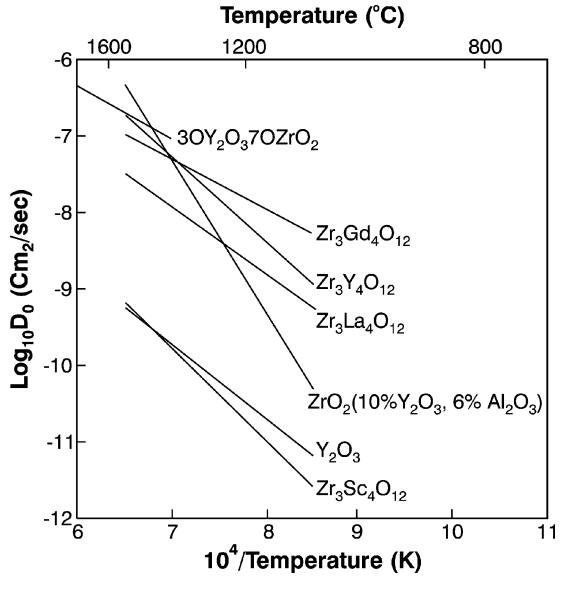

Figure 12 Oxygen diffusivity for ZrO_2-rare earth oxide ceramics.

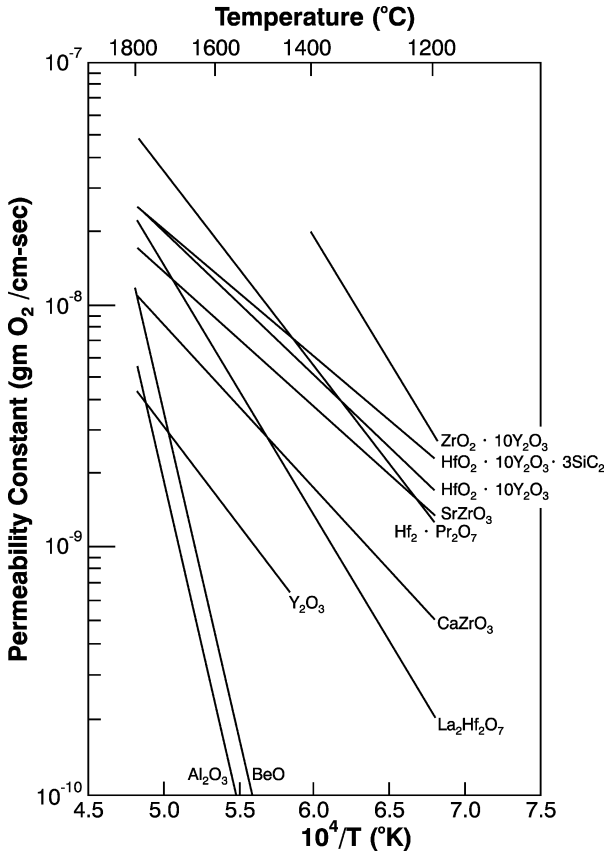

Figure 13 Oxygen permeability constants for oxide ceramics with pyrochlore structure.

hydrocarbon combustion [88]. A polished cross-section of HfC oxidized in arc-heater testing at 2700° for 30 s is shown in Fig. 14, revealing the porous oxide scale [89]. Vapor pressures for CO formed at the ZrC-ZrO_2 and HfC-HfO_2 interfaces have been calculated and exceed 1.01×10^5 Pa at 1730°C for both systems [90]. Thus, the carbides of Zr and Hf are compromised by the high vapor pressures formed at the oxide-carbide interface. The formation of porous scales was similarly observed for the nitrides.

The formation of Zr and Hf oxycarbide intermediate phases in the ZrC-ZrO_2 and HfC-HfO_2 systems have been reported, as the primary oxygen barriers [91, 92] and as stable phases in themselves [93, 94]. Hafnium carbide was reported as exhibiting superior oxidation resistance to HfB_2 at 1400 to 2100°C [91], but is based on furnace testing which biases the results unfavorably against the borides, as discussed previously. Stable oxycarbide phases have been reported for some rare earth metals, which suggests that rare earth additions may be employed to stabilize the oxycarbide phase in the scale. It is suggested that scandium (or ScC_{1-x}) be investigated since Sc has the same atomic radius as Zr or Hf and should exhibit high solubility into the base materials ZrC or HfC. Carbon interlayers, forming between the oxide and the base material, have also been reported for these carbides [95, 96].

Finally, the carbides are vulnerable to forming a powdery and non-adherent oxide scale below approximately 1700°C, which has been attributed to an inability to sinter at these temperatures [29, 97, 98]. Sintered and zone-melted samples exhibited low-temperature

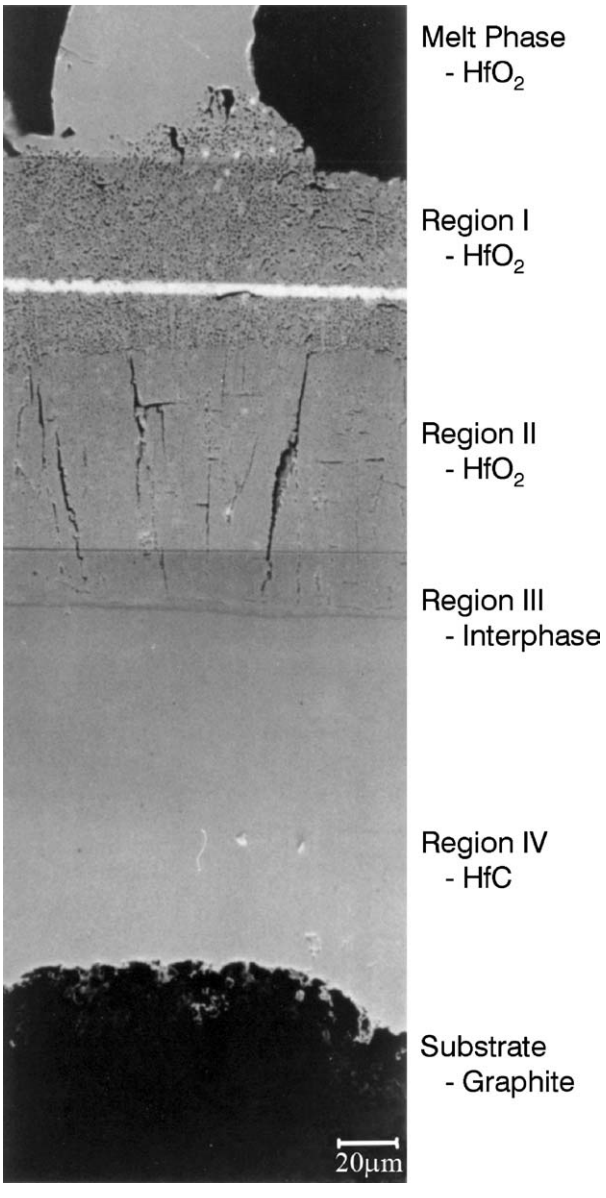

Figure 14 Microstructure (polished cross-section) of HfC arc-heater-oxidized at 2700°C for 30 s.

catastrophic oxidation [30], while chemically vapor deposited (CVD) materials have exhibited protective scale formation [91]. The nature of the low temperature oxidation vulnerability is not understood at this time.

5. Oxidation studies—Glass scale modification

Oxidation behavior of non-oxide ceramics depends highly on the properties of the oxidation product and on the combination of physical and chemical processes taking place on the surface exposed to oxygen-containing atmosphere. In general, the chemical composition and structure of an oxidized surface define the oxidation stability of a ceramic material. Modification of the chemical composition of the oxide surface layer, leading to decreased inward diffusion of oxygen, is one of the efficient ways of controlling oxidation resistance of non-oxide ceramics. This modification can be accomplished by changing the bulk composition, or the surface of ceramics using CVD, ion implantation, "pack cementation", and other methods.

For example, the oxidation resistance of ZrB_2 ceramics was significantly improved by modifying the bulk composition with SiC leading to the formation of a protective surface layer of borosilicate glass during exposure to an oxygen-containing atmosphere [18, 20, 33, 34, 39, 84]. The research conducted at NSWCCD showed that a further improvement of the oxidation performance of ZrB_2-SiC ceramics (up to 1600°C to-date) can be accomplished by the addition of CrB_2, TiB_2, TaB_2, NbB_2, and VB_2 [99]. Oxidation of the modifying diborides resulted in the formation of corresponding oxides in the surface borosilicate glass. It should be emphasized that the oxidation resistance of all of the modifying diborides (alone) is much lower than that of the ZrB_2 and HfB_2 ceramics [14, 22].

It is known from the literature that borate and silicate glasses containing Group IV-VI transition metal oxides show strong tendency to phase separation (immiscibility) [100]. Systems exhibiting immiscibility are characterized by steeply rising liquidus temperatures and increased viscosity. An increase in the viscosity decreases the oxygen diffusion rate through the oxide surface scale based on the Stokes—Einstein relationship [101], which shows that diffusivity is inversely proportional to viscosity. Another potential benefit of increased viscosity as well as increased liquidus temperature is the suppression of boria evaporation from the glass. The oxide effectiveness in enhancing immiscibility increases with increasing metallic element cation field strength, z/r^2, where z is the valence and r is the ionic radius [100–103]. Since the cation field strengths of Ti, Nb, Ta, Mo, Cr, and V are higher than that of Zr, these elements can be effective in promoting phase separation of the borosilicate glass formed on the surface of the ZrB_2-SiC ceramics. The concept of phase separation as a controlling factor in the oxidation protection of non-oxide ceramics is unique and has not been discussed in the literature.

The modifying diboride additives were introduced into the ZrB_2-SiC ceramics in the amounts of 2–20 mol% as a substitution for ZrB_2. The molar ratio of ZrB_2 to SiC in all materials was maintained at 2 (25 vol% SiC). The ceramics were prepared by hot pressing starting mixtures, consisting of ZrB_2, SiC, and modifying additives, at 2100°C and 20 MPa for 0.5 h. Oxidation experiments were conducted by heating the samples in a furnace in air at 1200–1600°C, typically for 2 h. The samples were placed into the furnace at the test temperatures and then air quenched after the hold. Quenching of the samples was conducted to retain the high temperature condition of the surface layer for analysis. Additionally, the oxidation of the samples was characterized by thermal gravimetric analysis (TGA) during 5 h isothermal heating at different temperatures in the air-simulating oxygen/argon mixture. The composition and structure of the surface and cross-section of the oxidized ceramics were evaluated using X-ray diffraction (XRD), SEM, and EDS.

Fig. 15 shows the results of isothermal (5 h) TGA heating at 1300°C of ZrB_2-SiC ceramics modified with

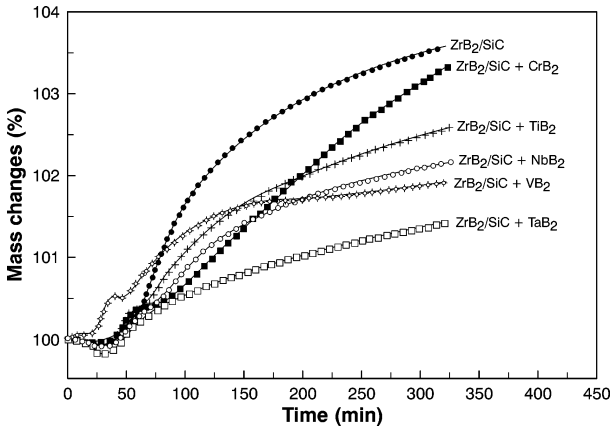

Figure 15 Isothermal TGA oxidation at 1300°C of ZrB_2/SiC ceramics modified with 10 mol% CrB_2, TiB_2, NbB_2, VB_2, and TaB_2.

10 mol% of CrB_2, NbB_2, TaB_2, TiB_2 and VB_2. The presence of the corresponding oxides in the oxidized surface layer improved the oxidation performance of the baseline material. The lowest weight gain during oxidation was observed for the ceramics containing TaB_2. The thickness of the oxidized layer of this sample was less than half of that for the baseline material [99]. The weight gain decreased in the sequence of the modifying additives: CrB_2, TiB_2, NbB_2, VB_2, and TaB_2, correlating well with the cation field strength for Cr^{+3}, Ti^{+4}, Nb^{+5}, V^{+4}, and Ta^{+5} [99].

SEM studies showed the evidence of high-temperature phase separation on the surfaces of all the modified samples after both TGA and furnace oxidation tests. Fig. 16a shows the surface of the sample containing 10 mol% TaB_2after the TGA oxidation test. The presence of large (more than 100 μm) droplets of borosilicate glass periodically distributed in a partially crystallized glassy matrix is an indication of high temperature glass phase separation. The matrix glass is enriched with Zr and Ta (from the EDS analysis data). X-ray diffraction of the whole surface of the oxidized sample showed the presence of ZrO_2 along with a small amount Ta $Zr_{2.75}O_8$ with melting temperature above 1700°C.

The CrB_2-containing ceramics (Fig. 16b) exhibited multiple phase separation after furnace oxidation at 1500°C, with shells around chromium-rich droplets which is the consequence of incomplete diffusion during cooling. A periodic pattern of crystals on the surface of ceramics modified with NbB_2 (Fig. 16c) implies the existence of glasses of different compositions at the test temperature. X-ray diffraction analysis of the surface showed that the crystalline phase is $Nb_2Zr_6O_{17}$ with a melting temperature about 1500°C. The glassy phase contains only small amounts of Nb and Zr (from EDS analysis). The presence of glass immiscibility is also observed on the surface of the ceramics modified with 5 mol% VB_2 after TGA oxidation at 1300°C (Fig. 16d). Circular microcracking around droplets in this sample

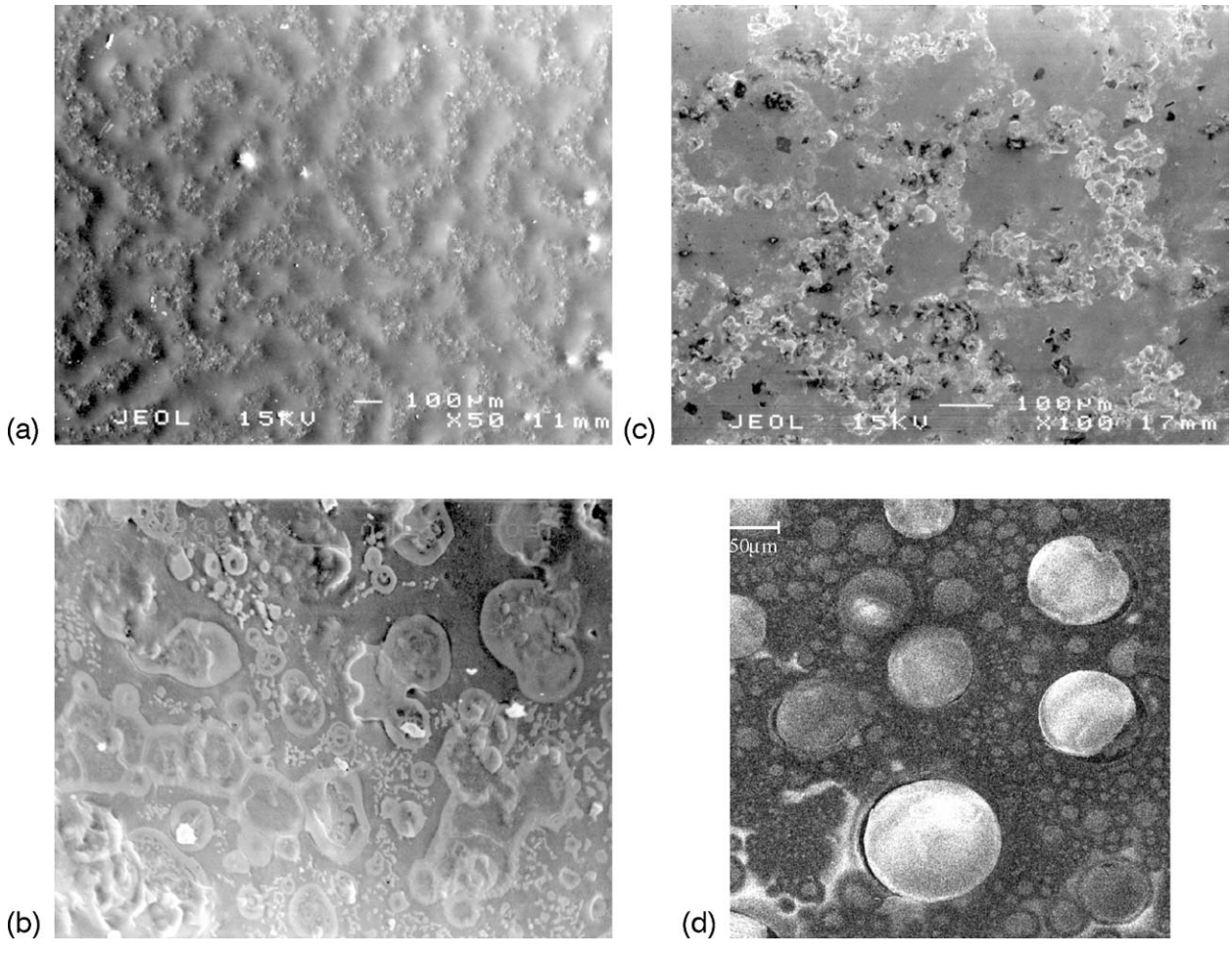

Figure 16 SEM micrographs of the surface of oxidized ZrB_2-SiC ceramics modified with: (a) TaB_2, (b) CrB_2, (c) NbB_2, and (d) VB_2.

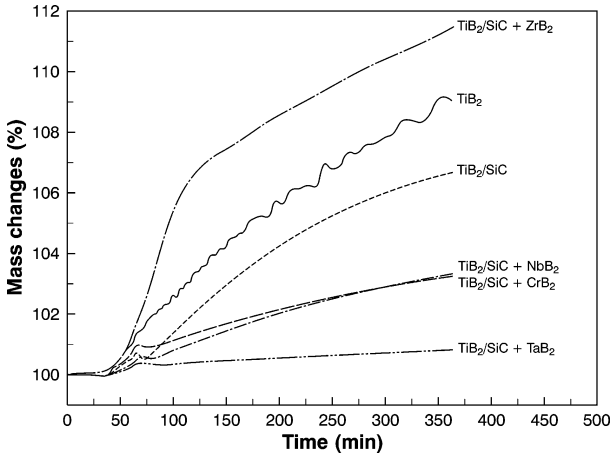

Figure 17 Isothermal TGA oxidation at 1300°C of TiB_2 and TiB_2-SiC ceramics modified with 20 mol% ZrB_2, CrB_2, NbB_2, and TaB_2.

can be attributed to compositional differences resulting in thermal expansion coefficient mismatch and leading to the development of strain and cracking during cooling. X-ray diffraction showed the presence of V_7O_{13} in addition to ZrO_2 on the surface of the oxidized VB_2-containing sample.

The discovered correlation between oxidation resistance of ZrB_2 and the presence of phase separation in the surface protective glass was successfully applied to improve the oxidation performance of CrB_2, TiB_2, TaB_2, NbB_2, ZrB_2-Si_3N_4, Ti_3SiC_2, and Si_3N_4 ceramics. The major results for the TiB_2, Ti_3SiC_2, and Si_3N_4 ceramics are discussed below.

The oxidation behavior of the TiB_2 ceramics modified with SiC and 5–20 mol% CrB_2, NbB_2, TaB_2, and ZrB_2 was evaluated [104]. The ceramics were prepared by hot pressing starting mixtures consisting of TiB_2, SiC, and diboride modifiers at 2100°C and 20 MPa for 0.5 h. Both furnace heating and TGA were used to characterize the oxidation resistance of the ceramics. The data show that the TiB_2-SiC ceramics containing TaB_2, NbB_2, and CrB_2 have the best oxidation performance at all temperatures and additive contents. Fig. 17 presents the results of isothermal TGA heating at 1300°C. The addition of ZrB_2 led to the decrease in oxidation resistance, especially, at 20% loading.

The effect of additives on the oxidation resistance of TiB_2 ceramics correlates with the cation field strength values for the elements being highest for Ta and Nb. The presence of Zr^{+4} oxide, with cation field strength lower than that of Ti^{+4}, led to the low protecting capabilities of the surface glass. If the rule of mixtures, not cation field strength of elements, was a controlling factor in the properties of surface glass and its protective capabilities, the improvement in the oxidation behavior of TiB_2-SiC ceramics could be expected with the introduction of ZrB_2, having the highest oxidation resistance of all the studied diborides. The optical micrograph of the surface of the CrB_2-containing ceramics (Fig. 18) clearly shows the immiscibility of the glass with the Cr_2O_3-rich green areas and TiO_2-rich brown areas.

The Ti_3SiC_2 ceramics recently attracted considerable attention because of their unique microstructure resulting in the exceptional combination of properties such as a high melting point, high fracture toughness and thermal shock resistance, plasticity at elevated temperatures, high modulus, low hardness, easy machinability, and self-lubrication [105–107]. These properties make the Ti_3SiC_2 ceramics of very high practical importance in numerous applications. However, these ceramics experience significant oxidation at temperatures above 1000°C preventing their high-temperature application

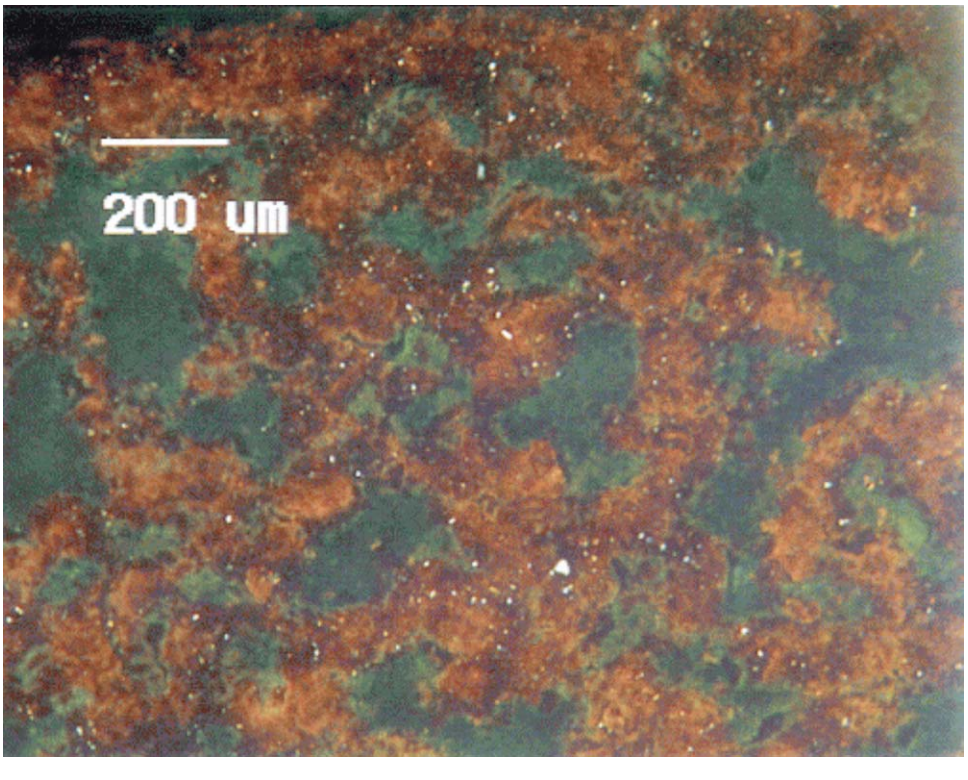

Figure 18 Optical micrograph of the surface of TiB_2-SiC ceramics containing 20 mol% CrB_2 after oxidation at 1200°C for 2 h.

in oxidizing environments. The modification of the ceramics with 10 mol% of TaB_2, ZrB_2, CrB_2, NbB_2, and VB_2 was undertaken to create phase-separated borosilicate glass on the surface of the ceramics and, thus, increase their oxidation resistance.

The Ti_3SiC_2 ceramics were synthesized and densified by reactive hot-pressing at 1500°C and 20 MPa for 1 h in He using the novel displacement reaction:

$$Ti_5Si_3 + 4TiC + 2C \rightarrow Ti_3SiC_2$$

The additives were introduced in the starting Ti_5Si_3-TiC-C mixtures. The samples were oxidized during air-furnace heating at 1000 to 1500°C, typically for two hours. The hot-pressed ceramics were fully dense and contained Ti_3SiC_2, small amounts of TiC, and additional phases associated with the additives. The SEM micrographs (Fig. 19a) show the presence of high aspect ratio plate-like grains, which define the mechanical behavior of the ceramics [105–107]. The additives (TaB_2 in Fig. 19b) did not noticeably change the microstructure of the baseline material.

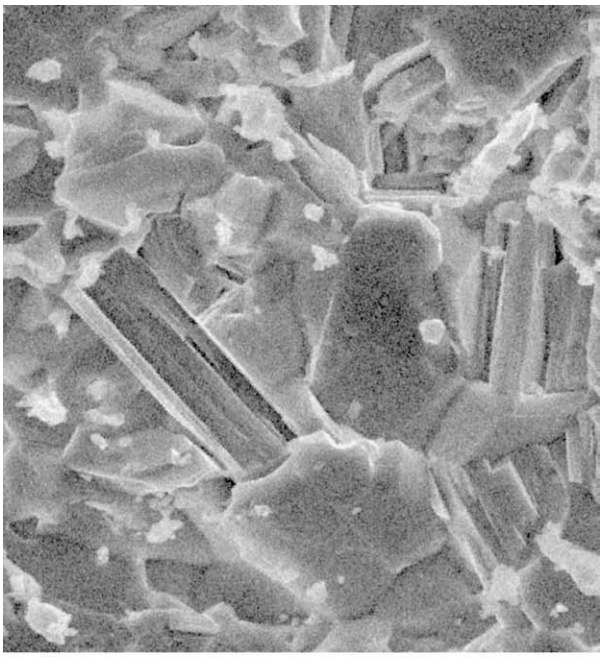

(a)

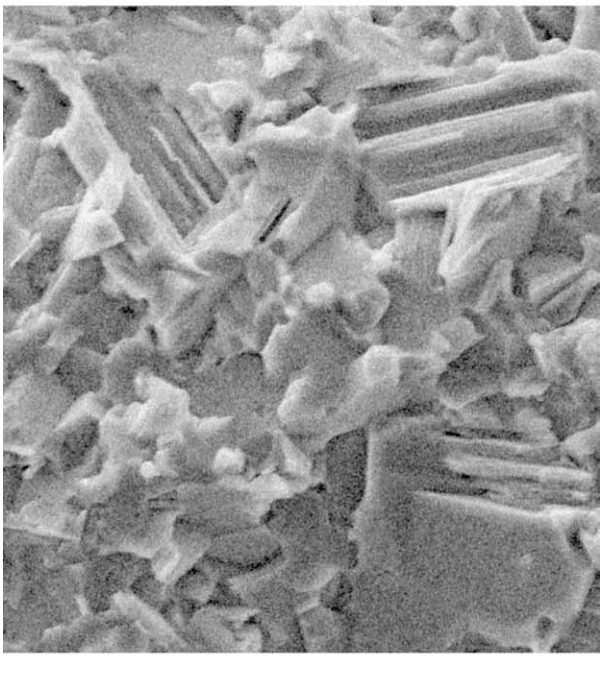

(b)

Figure 19 SEM micrographs of the fracture surface of Ti_3SiC_2 ceramics: (a) baseline Ti_3SiC_2 and (b) Ti_3SiC_2 modified with 10 mol% TaB_2.

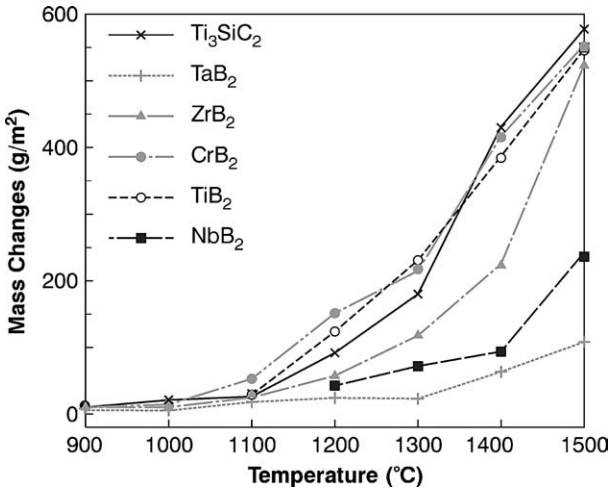

Figure 20 Oxidation of Ti_3SiC_2 ceramics modified with 10 mol% TaB_2, ZrB_2, CrB_2, TiB_2, and NbB_2 during furnace heating for 2 h.

The unmodified ceramics started to oxidize substantially at 1100°C (Fig. 20). Of all the diboride additives, NbB_2 and, especially, TaB_2 significantly improved the oxidation behavior of the ceramics. After 2 h oxidation at 1400°C, the weight gain was 430 g/m^2 for the baseline ceramics compared to 60 g/m^2 for the ceramics containing 10 mol% TaB_2. After heating at 1300°C the thickness of the oxidized layer was about 250 and 50 μm for the baseline and 10 mol% TaB_2—modified ceramics, respectively.

The microstructure of the oxidized surfaces of the baseline and TaB_2-modified ceramics (Fig. 21) is notably different. A bimodal distribution of the TiO_2 crystals with significantly different morphology and size is observed in the TaB_2-containing sample. The bimodal distribution and clustering of these crystals are probably an indication that crystallization occurred from immiscible glasses of different composition during high-temperature exposure. The pronounced effect of TaB_2 and NbB_2 forming corresponding oxides in the glass is related to the highest cation field strength of Nb and Ta compared to all other elements tested.

Silicon nitride is one of the most promising candidates for high-temperature structural applications, such as hot section components for advanced gas turbines and high-efficiency microturbines. High-temperature applications of Si_3N_4 ceramics depend, to a very high degree, on their behavior in corrosive environments and, primarily, on their resistance to oxidation. The effect of transition-metal diborides (CrB_2, TaB_2, and ZrB_2) was studied on the oxidation behavior and microstructure of oxidized Si_3N_4 ceramics containing 5 wt% Y_2O_3 and 2 wt% Al_2O_3 as sintering aids [108]. The ceramics were hot-pressed at 1825°C and 20 MPa

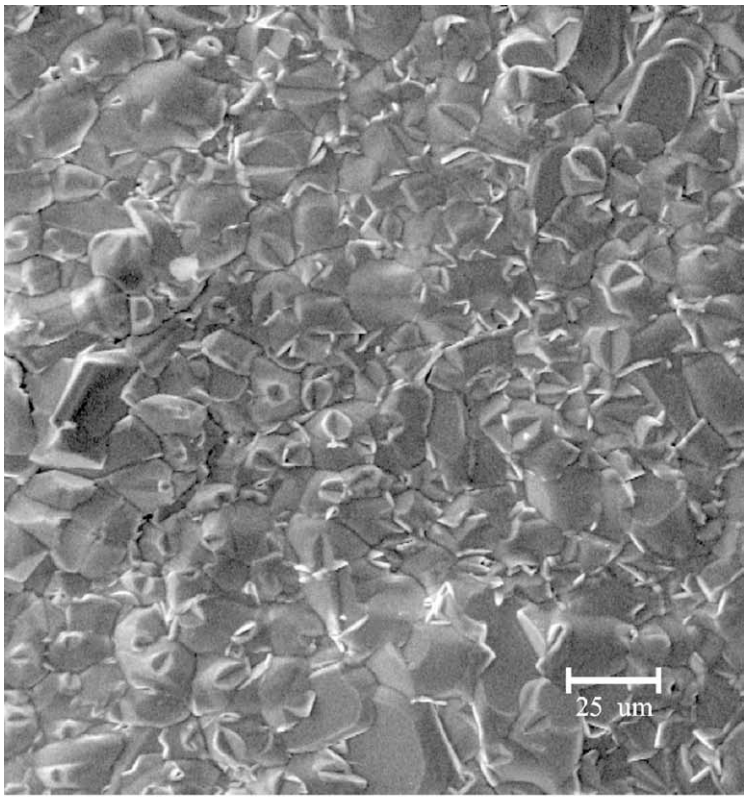

(a)

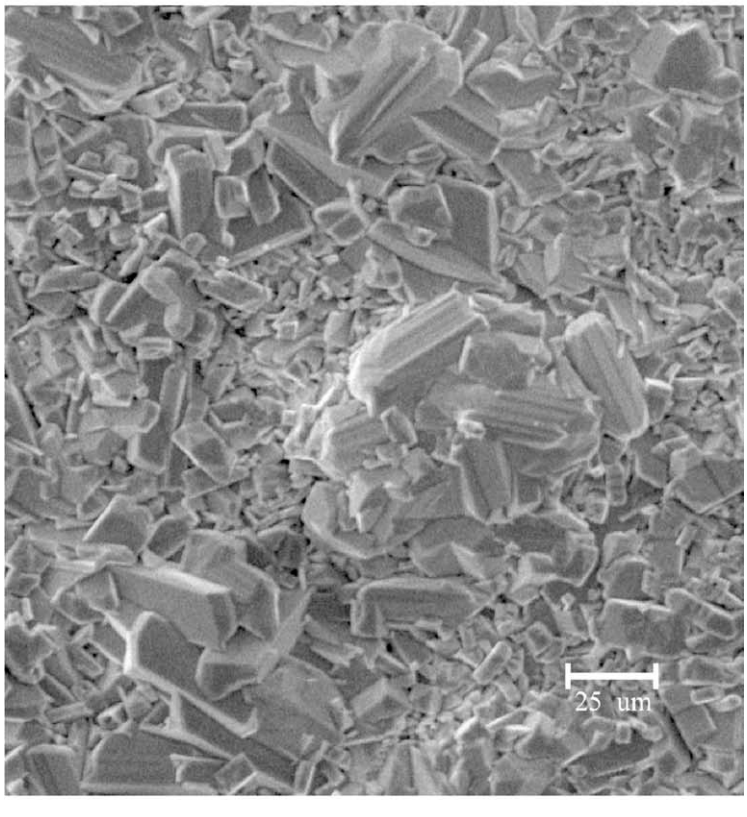

(b)

Figure 21 SEM micrographs of the surface of Ti_3SiC_2 ceramics after oxidation at 1200°C for 2 h: (a) baseline Ti_3SiC_2 and (b) Ti_3SiC_2 modified with 10 mol% TaB_2.

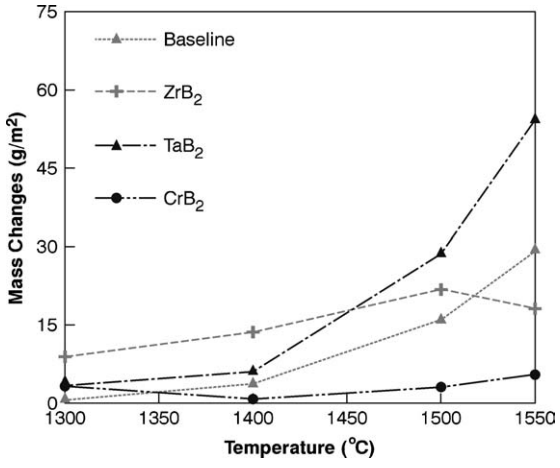

Figure 22 Oxidation of Si_3N_4 ceramics modified with 10 mol% ZrB_2, TaB_2, and CrB_2.

in He for 1 h. The oxidation behavior was characterized after furnace heating at 1200–1600°C in air.

Fig. 22 shows that no significant oxidation (weight change) was observed for any of the materials below 1300°C. However, above 1350°C, only CrB_2 significantly increased the oxidation resistance of the Si_3N_4 ceramics. The effect of the additives increases with increasing temperature. The SEM observations showed that the oxidized surface of the CrB_2-modified ceramics is almost fully crystallized, while the surface of the baseline ceramics is covered by a poorly crystallized, phase-separated glass (Fig. 23). The XRD analysis identified α-cristobalite as the only crystalline phase on the surface of the baseline material. In contrast, yttrium disilicate (monoclinic β-$Y_2Si_2O_7$) together with a small amount of α-cristobalite were found on the surface of the Cr-containing material. No Cr-containing

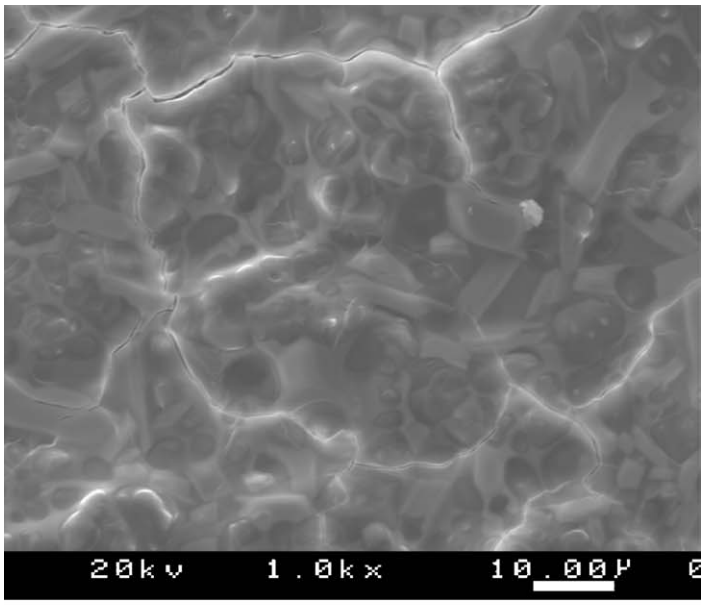

(a)

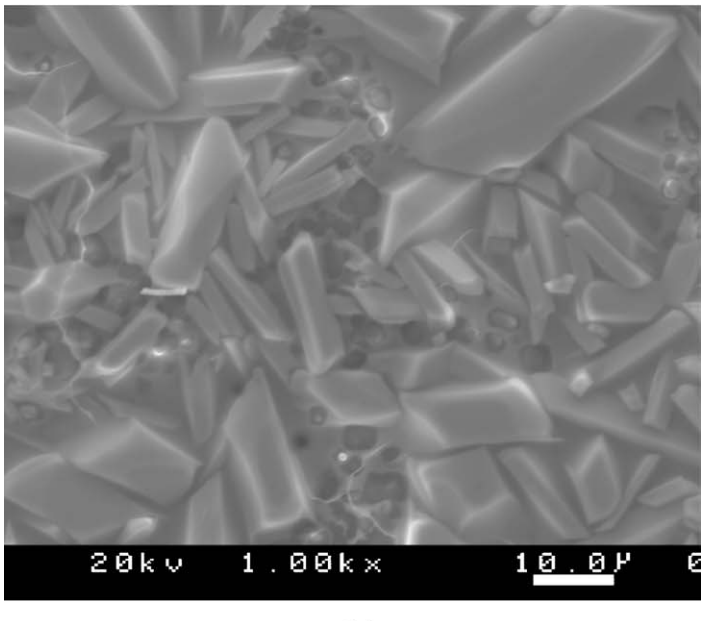

(b)

Figure 23 SEM micrographs of the surface of Si_3N_4 ceramics after oxidation at 1550°C for 2 h: (a) baseline Si_3N_4 and (b) Si_3N_4 modified with 5 vol% CrB_2.

compounds were detected, however, on the surface of the materials by either EDS or XRD.

It is hypothesized that chromium oxide present in the glass during oxidation additionally contributes to phase separation in the glass with the formation of a B-O-Si droplet phase and a Al-Y-Cr-Si-B-O matrix phase. Homogeneous nucleation and the formation of Cr_2O_3 crystallization centers occur in the matrix phase, followed by the catalytic crystallization of elongated $Y_2Si_2O_7$ grains, while a small amount of fine cristobalite grains crystallizes from the droplet phase. The high concentration of $Y_2O_3 \cdot 2SiO_2$ crystals (melting temperature 1775°C) on the surface of the Cr-containing ceramics provides effective oxidation protection during exposure to oxidizing atmosphere. The highest oxidation resistance was shown by the ceramics containing less than 5 vol% CrB_2.

The results of this research clearly showed that the oxidation resistance of non-oxide ceramics can be significantly enhanced by compositional design leading to the formation of a surface layer of immiscible multicomponent glass. The resulting increased liquidus temperatures and viscosities, as well as decreased oxygen diffusivities, in the immiscible glasses are considered responsible for the observed improvement in the oxidation resistance of the ceramics.

The difference in the immiscibility and the corresponding oxidation behavior for different ceramics and modifying additives is a function of the oxidation state of elements in a particular glass, which highly affects their cation field strength and, consequently, the tendency of the glass toward phase separation. For example, Cr exhibited different oxidation states depending on the base ceramic material, and test temperature and atmosphere (TGA versus furnace oxidation). The presence of CrO_2 was detected in the oxidation layer of several samples. The effective cation field strength of Cr^{+4} is much higher than Cr^{+3} (1322 compared to 793 nm^{-2}) while that of Ta^{+5} is constant at 1220 nm^{-2}. This offers an explanation for the alternating effectiveness of Ta and Cr modifiers in enhancing oxidation resistance.

6. Conclusions

High vapor pressures at the metal-metal oxide interfaces of the slow-growing oxides (SiO_2, Al_2O_3, Cr_2O_3, BeO) are disruptive at 1800°C or below. The high interfacial vapor pressures of these systems primarily result from the system thermochemistry and are only secondarily dependent on the oxidation kinetics. Among these oxides, a glass-forming SiO_2 scale exhibits significantly higher temperature capability, compared to materials which form a crystalline Al_2O_3, Cr_2O_3, or BeO scale, due to the greater structural tolerance of glass to high interfacial vapor pressures.

Materials that form a multi-component oxide scale, composed of a refractory oxide skeleton and an amorphous (glass) oxide component, provide good oxidation performance at hypersonic use temperatures up to, and above, 2000°C. This multi-component oxide system is the only structure known at this time that mitigates, or recovers from, high interfacial vapor pressures. The oxidation resistance of ZrB_2-SiC and other non-oxide materials is improved, to at least 1600°C, by compositional modifications with transition metal additives that promote immiscibility in the glass component of the scale. The oxidation mechanisms of materials forming this scale structure (e.g., ZrB_2-SiC) are still not well-understood despite 40 years of research.

Acknowledgements

Sustained support by Dr. Stephen Fishman of the Office of Naval Research, and by the Naval Surface Warfare Center (Dahlgren and Carderock Divisions), is gratefully acknowledged. The authors would like also to thank Dr. E. Opila for insightful editing contributions, Dr. B. Varshal for valuable discussions on glass immiscibility issues, Dr. D. Dallek for performing TGA tests, and intern students for participation in the experiments. One of the authors (M.M.O.) expresses deep appreciation for the privilege to learn metallurgical thermodynamics from Professor Robert Rapp of Ohio State University. The errors are the author's, however.

References

1. M. A. LEVINSTEIN, in Proceedings of Metallurgical Society Conference on Refractory Metals and Alloys, Chicago, April 1962, edited by M. Semchysen and I. Perlmutter (Interscience Publishers, New York, London, 1963) p. 269.
2. "High-Temperature Inorganic Coatings," edited by J. Huminik (Reinhold, New York, 1963).
3. "Coatings of High-Temperature Materials," edited by H. H. Hausner (Plenum, New York, 1966).
4. "Protective Coatings on Metals," edited by G. V. Samsonov, English Translation (Consultants Bureau, New York, 1969) Vol. 1.
5. "Protective Coatings on Metals," edited by G. V. Samsonov, English Translation (Amerind, New Delhi, 1984) Vol. 6.
6. C. M. PACKER, in "Oxidation of High-Temperature Intermetallics," edited by T. Grobstein and J. Doychak (TMS, 1988) p. 235.
7. G. H. MEIER, in "Oxidation of High-Temperature Intermetallics," edited by T. Grobstein and J. Doychak (TMS, 1988) p. 1.
8. T. GROBSTEIN and J. DOYCHAK (eds.), "Oxidation of High-Temperature Intermetallics" (TMS, 1988).
9. K. J. ZEITSCH and J. M. CRISCIONE, Technical Report WADD TR 61-72, Vol. XXX, AFML WPAFB, April 1964.
10. D. A. SCHULZ *et al.*, Technical Report WADD TR 61-72, Vol. XXXIV, AFML WPAFB, July 1964.
11. D. A. KRIVOSHEIN *et al.*, *Sov. Powd. Met. Met. Cer.* **6** (1978) 460.
12. R. KIESSLING, *Acta Chem. Scand.* **4** (1950) 160.
13. B. POST *et al.*, *Acta Met.* **2** (1954) 20.
14. R. STEINITZ *et al.*, *Trans. AIME, J. Metals* **4** (1952) 983.
15. L. KAUFMAN and E. CLOUGHERTY, Technical Report RTD-TDR-63-4096, Part 1, AFML, WPAFB, OH, Dec. 1963.
16. L KAUFMAN and E. CLOUGHERTY, Technical Report RTD-TDR-63-4096, Part 2, AFML, WPAFB, OH, Feb. 1965.
17. E. V. CLOUGHERTY *et al.*, in Proceedings of the 15th SAMPE Symposium, Vol. 15 (1969) p. 297.
18. J. R. FENTER, *SAMPE Quar.* **2** (1971) 1.
19. E. V. CLOUGHERTY *et al.*, Technical Report AFML-TR-68-190, AFML, WPAFB, OH, July 1968.
20. E. V. CLOUGHERTY *et al.*, *Trans. AIME* **242** (1968) 1077.
21. L. KAUFMAN and H. NESOR, Technical Report AFML-69-84, AFML, WPAFB, OH, March 1970.
22. L. A. MCCLAINE (ed.), Technical Report ASD-TDR-62-204, AFML, WPAFB, OH, 1962–1964.
23. J.B. BERKOWITZ-MATTUCK, Technical Report ASD-TDR-62-203, AFML, WPAFB, OH, 1962/1963.

24. P. T. B. SHAFFER, *Cer. Bull.* **41** (1962) 96.
25. H. PASTOR and R. MEYER, *Rev. Int. Htes Temp. et Refract.* **II** (1974) 41.
26. V. A. LAVRENKO, *et al.*, *Sov. Powd. Met. and Met. Cer.* **21** (1982) 471.
27. L. A. MCCLAINE (ed.), Technical Report ASD-TDR-62-204, Part II, AFML, WPAFB, OH, May 1963.
28. F. H. BROWN, Progress Report No. 20-252, Jet Propulsion Laboratory, Pasadena, CA, 25 Feb 1955.
29. A. K. KURIAKOSE and J. L. MARGRAVE, *J. Electrochem. Soc.* **111** (1964) 827.
30. J. B. BERKOWITZ-MATTUCK, *ibid.* **113** (1966) 908.
31. L. A. MCCLAINE (ed.), Technical Report ASD-TDR-62-204, Part III, AFML, WPAFB, OH, April 1964.
32. L. KAUFMAN *et al., Trans. AIME* **239** (1967) 458.
33. H. C. GRAHAM *et al.*, in "Ceramics in Severe Environments," edited by W. W. Kriegel and H. Palmour (Plenum Press, NY, 1971).
34. W. C. TRIPP and H. C. GRAHAM, *Solid State Science*, **118** (1971) 1195.
35. R. F. VOITOVICH and E. A. PUGACH, *Sov. Powd. Met. Met. Cer.* **147** (1975) 70.
36. E. I. GOLOVKO and R. F. VOITOVICH, *ibid.* **190** (1978) 77.
37. A. LEBUGLE and C. MENTEL, *Rev. int. Htes. Temp. et Refract.* **11** (1974) 321.
38. J. W. HINZE *et al., J. Electrochem. Soc.* **122** (1975) 1249.
39. W. C. TRIPP *et al.*, *Ceram. Bull.* **52** (1973) 612.
40. M. C. JISCHKE, *Proc. Okla. Acad. Sci.* **53** (1973) 81.
41. E. V. CLOUGHERTY *et al.*, in Proceedings of the 15th National SAMPE Symposium (1969) Vol. 15, p. 297.
42. L. KAUFMAN, in Proceedings of AIAA Advanced Space Transportation Meeting (AIAA, NY, 1970) Paper 70-278.
43. J. D. BUCKLEY, Technical Report NASA TN D-4231, NASA, Wash DC, Oct. 1967.
44. M. L. HILL, in Proceedings of the AIAA/ASME 8th Conference on Structures, Structural Dynamics, and Materials (AIAA, NY, 1967) p. 248.
45. D. R. GASKELL, in "Introduction to Metallurgical Thermodynamics" (Hemisphere, New York, 1981).
46. C. H. P. LUPIS, in "Chemical Thermodynamics of Materials" (Elsevier, New York, 1983).
47. "Thermodynamics of Certain Refractory Compounds," edited by H. Schick (Academic Press, New York and London, 1966) Vol. II.
48. "JANAF Thermochemical Tables," 2nd ed., edited by D. R. Stull and H. Prophet (U.S. Dept. of Commerce, National Bureau of Standards, Washington D. C., 1971).
49. L. B. PANKRATZ, "Thermodynamic Properties of Elements and Oxides, Bulletin 672 (U.S. Dept. of the Interior, Bureau of Mines, 1982).
50. O. KNACKE *et al.*, in "Thermochemical Properties of Inorganic Substances" (Springer-Verlag, Berlin, 1991).
51. M. S. CHANDRASEKHARAIAH *et al., J. Less-Common Met.* **80** (1981) 9.
52. A. OLIVEI, *ibid.* **29** (1972) 11.
53. H. JEHN *et al.*, *ibid.* **100** (1984) 321.
54. P. KOFSTAD, "High-Temperature Oxidation of Metals" (John Wiley & Sons, Inc., New York, London, Sydney, 1966).
55. C. T. SIMS *et al., Trans. AIME* (1955) 168.
56. C. T. SIMS *et al.*, Technical Report WADC 56-319 ASTIA Document 110596 (1956).
57. W. W. SMELTZER and M.T. SIMNAD, *Acta Metallurgica* **6** (1957) 328.
58. R. E. PAWEL and J. J. CAMPBELL, *J. Electrochem. Soc.* **128** (1981) 1999.
59. B. E. DEAL and A. S. GROVE, *J. Appl. Phys.* **36** (1965) 3770.
60. C. S. GIGGINS and F. S. PETTIT, *J. Electrochem. Soc.* **118** (1971) 1782.
61. W. C. HAGEL, *Trans. ASM* **56**(1963) 583.
62. J. BOOKER, R. M. PAINE and A. J. STONEHOUSE, Technical Report WADD TR 60-889 (1961).
63. J. BOOKER, R. M. PAINE and A. J. STONEHOUSE, Technical Report WADD TR 60-889 (1962).
64. R. M. PAINE, A. J. STONEHOUSE and W. W. BEAVER, *Corrosion* **20** (1964) 307.
65. N. S. JACOBSON, *J. Amer. Ceram. Soc.* **76** (1993) 3.
66. J. R. STRIFE and J. E. SHEEHAN, *Cer. Bull.* **67** (1988) 369.
67. H. H. KELLOGG, *Trans. Met. Soc. AIME* **236** (1966) 602.
68. E. A. GULBRANSEN and S. A. JANSSON, in "Oxidation of Metals and Alloys" (ASM, Metals Park, OH, 1971) p. 63.
69. C. WAGNER, *J. Appl. Phys.* **29** (1958) 1295.
70. V. L. K. LOU, T. E. MITCHELL and A. H. HEUER, *J. Amer. Ceram. Soc.* **68** (1985) 49.
71. A. H. HEUER and V. L. K. LOU, *ibid.* **73** (1990) 2789.
72. E. A. GULBRANSEN, K. F. ANDREW and F. A. BRASSART, *J. Electrochem. Soc.* **113** (1966) 834.
73. G. R. ST PIERRE, in Proceedings of Conference on Gas-Solid Reactions in Pyrometallurgy, Purdue U., April 1986.
74. J. W. HINZE and H. C. GRAHAM, *J. Electrochem. Soc.* **123** (1976) 1066.
75. G. H. SCHIROKY, *Adv. Ceram. Matls.* **2** (1987) 137.
76. W. L. VAUGHN and H. G. MAAHS, *J. Amer. Ceram. Soc.* **73** (1990) 1540.
77. G. H. MEIER, in "Oxidation of High-Temperature Intermetallics," edited by T. Grobstein and J. Doychak (TMS, 1988) p.1.
78. D. CAPLAN and G. I. SPROULE, *Oxidation of Metals* **9** (1975) 459.
79. R. A. RAPP, High Temperature Corrosion, ACS Course Notes, ACS, 1980, 60.
80. Z. ZHENG *et al.*, *J. Electrochem. Soc.* **137** (1990) 854.
81. Z. ZHENG *et al.*, *ibid.* **137** (1990) 2812.
82. L. KAUFMAN and H. NESOR, Technical Report AFML-69-84, Pt. III, Vol. III, AFML, WPAFB, OH, March 1970.
83. L. KAUFMAN and E. CLOUGHERTY, Technical Report RTD-TDR-63-4096, Part 2, AFML, WPAFB, OH, Feb. 1965.
84. I. G. TALMY, J. A. ZAYKOSKI and M. M. OPEKA *Ceram. Eng. Sci. Proc.* **19** (1998) 105.
85. W. W. WEYL and E. C. MARBOE, in "The Constitution of Glasses—A Dynamic Interpretation" (Interscience, New York, 1962) p. 618.
86. R. TURCOTTE *et al.*, Technical Report WL-TR-91-4059, AFML, WPAFB, OH, March 1992.
87. E. L. COURTWRIGHT et al., Technical Report WL-TR-91-4061, AFML, WPAFB, OH, Sept. 1992.
88. Unpublished data.
89. J. S. EVANGELIDES, Unpublished materials analyses.
90. J. B. BERKOWITZ-MATTUCK, Technical Report ASD-TDR-62-203 Part II, AFML, WPAFB, OH, March 1963.
91. C. B. BARGERON and R. C. BENSON, *Surf. Coat. Tech.* **36** (1988) 111.
92. C. B. BARGERON et al., *JHU APL Tech. Digest* **14** (1193) 29.
93. J. HENNEY and J. W. S. JONES, in "Special Ceramics 1964," edited by P. Popper (Academic Press, London and New York, 1965) p. 35.
94. V. A. ZHILYAEV *et al.*, *Sov. Powd. Met. Met. Cer.* **11** (1972) 632.
95. R. F. VOITOVICH and E. A. PUGACH, *ibid.* **12** (1973) 916.
96. E. J. WUCHINA and M. M. OPEKA, *J. Electrochem. Soc.* **99**(38) (2000) 477.
97. G. R. HOLCOMB, "The High Temperature Oxidation of Hafnium Carbide," Ph.D. Thesis, Ohio State University, 1988.
98. E. L. COURTRIGHT *et al.*, *Oxidation of Metals* **36** (1991) 423.
99. I. G. TALMY *et al.*, in Proceedings of the International Symposium on "High Temperature Corrosion and Materials Chemistry III," edited by M. McNallan and E. Opila (The Electrochemical Society, Inc., Pennington, NJ, 2001) Vol. 2001-12, p. 144.
100. W. VOGEL, "Glass Chemistry," 2nd ed. (Springer-Verlag, New York, 1994).
101. P. W. ATKINS, in "Physical Chemistry" (Oxford University Press, 1978).
102. F. P. GLASSER, I. WARSHAW and R. ROY, *Phys. Chem. Glass.* **l** (1960) 139.
103. B. G. VARSHAL, *Glass Phys. Chem.* **19** (1993) 1.

104. J. A. ZAYKOSKI *et al*., *FY 2000 NSWC Res. Digest* (2000) 95.
105. M. W. BARSOUM and T. EL-RAGHY, *J. Amer. Ceram. Soc*. **79** (1996) 1953.
106. J. FRYT and L. STOBIERSKI, Trans Tech Pubs., Switzerland, (1997) p. 1608.
107. N. F. GAO, MIYAMOTO and D. ZHANG, *J. Mater. Sci*. **18** (1999) 4385.
108. I. G. TALMY *et al*., in Proceedings of the International Symposium on "High Temperature Corrosion and Materials Chemistry IV," edited by E. Opila, P. Hou, T. Maruyama, D. Shifler and E. Wuchina (The Electrochemical Society, Inc., Pennington, NJ, 2003) Vol. 2003-16, p. 361.

Received 28 February
and accepted 29 April 2004